

# Stellar neutrino energy loss rates due to $^{24}\text{Mg}$ suitable for O+Ne+Mg core simulations

Jameel-Un Nabi\*

*Faculty of Engineering Sciences, GIK Institute of Engineering Sciences and Technology, Topi 23640, Swabi, NWFP, Pakistan*

*Current Address: ICTP, Strada Costiera 11, 34014, Trieste, Italy*

Neutrino losses from proto-neutron stars play a pivotal role to decide if these stars would be crushed into black holes or explode as supernovae. Recent observations of subluminoous Type II-P supernovae (e.g., 2005cs, 2003gd, 1999br, 1997D) were able to rejuvenate the interest in 8-10  $M_{\odot}$  stars which develop O+Ne+Mg cores. Simulation results of O+Ne+Mg cores show varying results in converting the collapse into an explosion. The neutrino energy loss rates are important input parameters in core collapse simulations. Proton-neutron quasi-particle random phase approximation (pn-QRPA) theory has been used for calculation of neutrino energy loss rates due to  $^{24}\text{Mg}$  in stellar matter. The rates are presented on a detailed density-temperature grid suitable for simulation purposes. The calculated neutrino energy loss rates are enhanced up to more than one order of magnitude compared to the shell model calculations and favor a lower entropy for the core of these massive stars.

**PACS** numbers: 23.40.Bw, 21.60.Jz, 26.30.Jk, 26.50.+x

## I. INTRODUCTION

It is now more than forty years since Colgate & White [1] and Arnett [2] presented their classical work on energy transport by neutrinos and antineutrinos in non-rotating massive stars. Despite immense technological advancements in recent times, the explosion mechanism of core-collapse supernovae continues to challenge astrophysicists throughout the globe. When the iron core becomes unstable against the gravity force its inner portion undergoes homologous collapse whereas the outer portion collapses supersonically. The prompt shock that follows the bounce of the core stagnates (as it loses energy due to neutrino emission and endothermic dissociation of heavy nuclei falling through the shock) leading to a standing shock. Some additional source of energy is required to revitalize the postshock gas. One interesting mechanism to revive the shock was the "preheating" mechanism proposed by Haxton [3]. Haxton suggested that a significant fraction of the energy carried by the neutrinos could be utilized in preheating iron nuclei

---

\* author e-mail: jnabi00@gmail.com

outside the shock front rather than getting lost. This would lead to a reduction in the energy required from the shock wave to dissociate the infalling Fe, assisting the shock wave to retain more of its strength as it propagates through the iron core and thus increasing the chances of transforming the collapse into an explosion. However, the preheating mechanism continues to be debated and the part played by neutrinos in this scenario is far from being completely understood. Later, Bruenn and Haxton [4] worked on models simulating weak and strong shock cases and found out that in neither case is the energy transferred to the matter by neutrino-nucleus absorption significant in terms of preheating the infalling iron-like material. More recently, Langanke and collaborators [5] had some observations on the models of Bruenn and Haxton [4] and reported much larger preshock heating rates. They concluded that these rates act for too short a time to lead to consequences for shock propagation. Despite all this, the preheating mechanism in fact has been adopted by most coders, who are continually putting in more microphysics to make the simulations more realistic and there continues to be interest in this problem [6].

During the late stages of evolution, a star mainly loses energy through neutrinos and this process is fairly independent of the mass of the star. White dwarfs and supernovae, both have cooling rates largely dominated by neutrino production. Neutrinos are crucial to the life and afterlife of a supernova. It is natural to consider neutrino heating as a probable mechanism for shock revival as they dominate the energetics and dynamics of the post-bounce evolution. Having only weak interactions, they are nature's most efficient means of cooling, transporting along around 99% of the released gravitational energy. As such it is no wonder that astrophysicists find it a formidable task to simulate a 1% effect of explosion.

White dwarfs located in a binary system may end their lives in two possible ways. They may accrete from a companion and achieve the Chandrasekhar mass thereby triggering a thermonuclear runaway of the object and ultimately exploding as a Type Ia supernova. In this case no remnant is left behind. Alternatively these massive white dwarfs, for sufficiently high mass accretion rates, may allow the formation of O+Ne+Mg cores and due to the high prevailing central density (beyond  $10^{10} \text{ g cm}^{-3}$ ) experience rapid electron capture that lead to the collapse of the core. This is termed as accretion-induced collapse (AIC). The end product is a neutron star (in some double-degenerate scenario, two white dwarfs in a short-period binary system may eventually coalesce to form a massive white dwarf that exceeds the Chandrasekhar mass limit and in this case transition to a black hole is possible if the total proto-neutron star mass exceeds the general-relativistic limit for gravitational stability [7]). The AIC of white dwarfs represents one instance where a neutrino mechanism leads undoubtedly to a successful, albeit weak, explosion [8]. The authors in Ref. [8] argued that the neutrino mechanism can successfully power explosions of low-mass progenitors and

AICs due to the limited mantle mass and steeply declining accretion rate. The ultimate fate of these white dwarfs are dependent on many factors, e.g. temperature of the environment, the mass accretion rate on the newly formed white dwarf, the mass of each partner white dwarf [7] and rapid electron capture rates [8]. The occurrence rate of the AIC of white dwarfs is not determined reliably, and are not expected to occur more than once per 20 – 50 standard Type Ia events (see for example [7]).

Supernovae are also tipped in as probable sites for the r-process. The production site of the heavy r-process nuclei is associated with the accretion-induced collapse of an oxygen-neon-magnesium (O+Ne+Mg) white dwarf in a binary system (e.g. [9]) or Type-II supernovae from 8–10  $M_{\odot}$  (e.g. [10]). These 8–10  $M_{\odot}$  stars form an electron-degenerate O+Ne+Mg core that does not undergo further nuclear burning. A few collapse simulators (e.g. Hillebrandt et al. [11]) demonstrated that the collapsing O+Ne+Mg core explodes promptly. Others (e.g. Woosley and Baron [12]) showed that the shock generated at core bounce stalls rather than leading to a prompt explosion. Delayed explosion scenario of these cores was also reported (e.g. Mayle and Wilson [13]). Wheeler and collaborators [14] have suggested that the exploding O+Ne+Mg core could be a viable site for the r-process. However the question of whether O+Ne+Mg cores can explode hydrodynamically continues to be argued. For example, Gutiérrez et al. [15] argued that the abundance of  $^{24}\text{Mg}$  was considerably reduced in updated evolutionary calculations. However the procedure adopted by them was not fully consistent as they kept the ratio of oxygen to neon constant while parameterizing the abundance of  $^{24}\text{Mg}$ . Later Kitaura et al. [16] presented simulation result of these cores (keeping capture rates on  $^{24}\text{Mg}$  as a key ingredient) using an improved neutrino transport treatment. Their outcome was not a prompt but a delayed explosion.

A smaller iron core present at the onset of the core bounce as well as the smaller gravitational potential of the collapsing cores of a 8–10  $M_{\odot}$  star do favor a prompt explosion. What remains certain is that microscopic and reliable electron capture rates and neutrino energy loss rates are needed for a careful study of the late stages of the stellar evolution of 8–10  $M_{\odot}$  stars and can contribute effectively in the final outcome of the simulations of O+Ne+Mg cores on world’s fastest supercomputers.

Electron capture rates and the accompanying neutrino energy loss rates of matter in nuclear statistical equilibrium under conditions of high temperatures and densities are of prime importance in determining the equation of state of exploding stars. An accurate determination of neutrino emission rates is mandatory in order to perform a careful analysis of the final branches of star evolutionary tracks. A change in the cooling rates at the very last stages of massive star evolution could affect the evolutionary time scale and the configuration of iron core at the onset of the supernova explosion.

Compared to shell model calculations by Wildenthal et al. [17], the proton-neutron quasiparticle random phase approximation theory (pn-QRPA) gives similar accuracy in the description of light nuclei including beta-decay rates in *sd*-shell nuclide [18]. Nabi and Klapdor [19], later, calculated weak interaction rates for 709 nuclei with  $A = 18$  to 100 in stellar matter using the pn-QRPA theory. These included capture rates, decay rates, neutrino energy loss rates, probabilities of beta-delayed particle emissions and energy rate of these particle emissions (see also Refs. [20,21]). Since then these calculations were further refined with use of more efficient algorithms, incorporation of latest data from mass compilations and experimental values, and fine-tuning of model parameters (e.g. Refs. [22 – 25]).

The evolution of the stars in the mass range 8-10  $M_{\odot}$  develops central cores which are composed of  $^{16}\text{O}$ ,  $^{20}\text{Ne}$  and  $^{24}\text{Mg}$ . Oda et al. [26] pointed out three different series of electron capture in the O+Ne+Mg core of the 8-10  $M_{\odot}$  stars and placed them in the order of low threshold energy as  $^{24}\text{Mg} \rightarrow ^{24}\text{Na} \rightarrow ^{24}\text{Ne}$ ,  $^{20}\text{Ne} \rightarrow ^{20}\text{F} \rightarrow ^{20}\text{O}$ , and  $^{16}\text{O} \rightarrow ^{16}\text{N} \rightarrow ^{16}\text{C}$ . The first series was regarded most important as the trigger nucleus,  $^{24}\text{Mg}$ , has the lowest electron capture threshold. Oda and collaborators [26] actually renounced the last series in their calculations because of its high threshold energy which did not contribute significantly to the initiation of the collapse of the O+Ne+Mg core of the 8-10  $M_{\odot}$  stars.

The Gamow-Teller strength distributions in  $^{24}\text{Mg}$  and the calculation of electron capture rates on  $^{24}\text{Mg}$  using the pn-QRPA theory for O+Ne+Mg core simulations were presented earlier by Nabi and Rahman [23]. Here I present for the first time the pn-QRPA calculations of the neutrino and antineutrino energy loss rates due to  $^{24}\text{Mg}$  in stellar plasma on a detailed temperature-density grid suitable for the simulation codes of O+Ne+Mg cores. In order to further increase the reliability of the calculated neutrino energy loss rates, I have incorporated all measured excitation energies (along with their  $\log ft$  values) with definite spin and/or parity assignment, by either replacement (when they were within 0.5 MeV of each other) or manual insertion. The deformation parameter,  $\delta$ , is recently argued to be one of the most important parameters in QRPA calculations [27]. For the case of even-even nuclei, experimental deformations are available [28] and were employed in this work. All these steps were taken to ensure the most reliable calculation of pn-QRPA neutrino and antineutrino energy loss rates due to  $^{24}\text{Mg}$  in presupernova and supernova environment.

The paper is written as follows. Section II deals with the brief formalism of the pn-QRPA calculations. I present some of my calculated results in Section III. Comparisons with earlier calculations is also included in this section. I finally conclude in Section IV and at the end Table II presents the detailed calculation of neutrino and antineutrino energy loss rates due to  $^{24}\text{Mg}$  suitable for simulation codes.

## II. MODEL DESCRIPTION

I used the pn-QRPA theory with a separable interaction to calculate the neutrino and antineutrino energy losses in stellar matter. The Hamiltonian of the problem was taken to be of the form:

$$H^{QRPA} = H^{sp} + V^{pair} + V_{GT}^{ph} + V_{GT}^{pp}. \quad (1)$$

For the single-particle Hamiltonian,  $H^{sp}$ , the single particle energies as well as wave functions were calculated in the Nilsson model (which takes into account nuclear deformations). The BCS model was used to calculate the pairing force,  $V^{pair}$ . Two types of proton-neutron residual interactions were incorporated in these calculations namely the particle-hole,  $V_{GT}^{ph}$ , and the particle-particle,  $V_{GT}^{pp}$ , interaction. The two interactions (separable in form) were characterized by two interaction constants:  $\chi$  (for particle-hole interaction) and  $\kappa$  (for particle-particle interaction). In this work, the values of  $\chi$  and  $\kappa$  was taken as 0.001 MeV and 0.05 MeV, respectively. (The reader is referred to [18,29] for details of optimum selection of these parameters.) Other parameters required for the calculation of weak rates are the deformation, the pairing gaps, and the Q-value of the nuclear reactions. The calculated half-lives depend only weakly on the values of the pairing gaps [30]. Thus, the traditional choice of  $\Delta_p = \Delta_n = 12/\sqrt{A}(MeV)$  was applied in the present work. The deformation parameter is as an important parameter for QRPA calculations as pairing [27]. As such rather than using deformations from some theoretical mass models (as used in earlier calculations of pn-QRPA capture rates) the experimentally adopted value of the deformation parameters for  $^{24}\text{Mg}$ , extracted by relating the measured energy of the first  $2^+$  excited state with the quadrupole deformation, was taken from Raman et al. [28]. Q-values were taken from the recent mass compilation of Audi et al. [31].

An estimation of uncertainties of the model and theoretical errors is important to establish the reliability of the calculated rates. The uncertainties related to the pn-QRPA model was discussed in detail in Ref. [32]. There the accuracy of the pn-QRPA model was compared to the experimental data for both  $\beta^+$  and  $\beta^-$  directions (see Table I and Table II of Ref. [32]) and an estimation of theoretical errors was given. The decay rate of even-even nuclei generally exhibits more or less a smooth behavior with respect to the deformation parameter (see Fig.2 of Ref. [18] and discussions therein). The dependence of the half-life on the pairing gaps is small and rather smooth (see Fig. 3 of Ref. [18]). The half-lives are not very sensitive to a change of the Gamow-Teller interaction strength  $\chi$  within a reasonable range and the relationship is almost linear [18]. On the other hand for large values of  $\kappa$  the lowest eigenvalue becomes complex. This indicates the "collapse" of the QRPA model and it is crucial to avoid values of  $\kappa$  which lie beyond the collapse. The redistribution of the  $\beta$  strength and the reduction of the sum of the Gamow-Teller

strength lead to a nonlinear dependence of the calculated half-lives as a function of  $\kappa$  [29]. Figs. (7 – 10) of Ref. [29] show in detail how the observables of the pn-QRPA calculations vary with changes in  $\kappa$ . These analysis do explain that a small and acceptable change in the QRPA parameters does not have a dramatic dependence on the calculated rates.

The neutrino energy loss rates can occur through four different weak-interaction mediated channels: electron and positron emissions, and, continuum electron and positron captures. The neutrino energy loss rates were calculated using the formula

$$\lambda_{ij}^\nu = \left[ \frac{\ln 2}{D} \right] [f_{ij}^\nu(T, \rho, E_f)] \left[ B(F)_{ij} + \left( g_A/g_V \right)^2 B(GT)_{ij} \right]. \quad (2)$$

The value of  $D$  was taken to be 6295s [33] and the ratio of the axial vector to the vector coupling constant as -1.254 [34].  $B'_{ij}$ s are the sum of reduced transition probabilities of the Fermi  $B(F)$  and Gamow-Teller transitions  $B(GT)$ . The  $f_{ij}^\nu$  are the phase space integrals and are functions of stellar temperature ( $T$ ), density ( $\rho$ ) and Fermi energy ( $E_f$ ) of the electrons. They are explicitly given by

$$f_{ij}^\nu = \int_1^{w_m} w \sqrt{w^2 - 1} (w_m - w)^3 F(\pm Z, w) (1 - G_\mp) dw, \quad (3)$$

and by

$$f_{ij}^\nu = \int_{w_l}^\infty w \sqrt{w^2 - 1} (w_m + w)^3 F(\pm Z, w) G_\mp dw. \quad (4)$$

In above equation  $w$  is the total energy of the electron including its rest mass,  $w_l$  is the total capture threshold energy (rest+kinetic) for positron (or electron) capture.  $F(\pm Z, w)$  are the Fermi functions and were calculated according to the procedure adopted by Gove and Martin [35].  $G_\pm$  is the Fermi-Dirac distribution function for positrons (electrons).

$$G_+ = \left[ \exp \left( \frac{E + 2 + E_f}{kT} \right) + 1 \right]^{-1}, \quad (5)$$

$$G_- = \left[ \exp \left( \frac{E - E_f}{kT} \right) + 1 \right]^{-1}, \quad (6)$$

here  $E$  is the kinetic energy of the electrons and  $k$  is the Boltzmann constant.

For the decay channel Eqt. (3) was used for the calculation of phase space integrals. Upper signs were used for the case of electron emissions and lower signs for the case of positron emissions. Regarding the capture channels, I used Eqt. (4) for the phase space integrals keeping upper signs for continuum electron captures and lower signs for continuum positron captures.

The total neutrino energy loss rate per unit time per nucleus is given by

$$\lambda^\nu = \sum_{ij} P_i \lambda_{ij}^\nu, \quad (7)$$

where  $\lambda_{ij}^\nu$  is the sum of the electron capture and positron decay rates for the transition  $i \rightarrow j$  and  $P_i$  is the probability of occupation of parent excited states which follows the normal Boltzmann distribution.

On the other hand the total antineutrino energy loss rate per unit time per nucleus is given by

$$\lambda^{\bar{\nu}} = \sum_{ij} P_i \lambda_{ij}^{\bar{\nu}}, \quad (8)$$

where  $\lambda_{ij}^{\bar{\nu}}$  is the sum of the positron capture and electron decay rates for the transition  $i \rightarrow j$ .

The pn-QRPA theory allows a microscopic state-by-state calculation of both sums present in Eqs. (7) and (8). In other words the pn-QRPA theory calculates the GT strength distribution of all excited states of parent nucleus in a microscopic fashion. This feature of the pn-QRPA model greatly increases the reliability of the calculated rates in stellar matter where there exists a finite probability of occupation of excited states. Further the pn-QRPA theory can handle any arbitrarily heavy system of nucleons since the calculation is performed in a luxurious model space of up to 7 major oscillator shells.

Details of the calculations of phase space integrals and reduced transition probabilities can be found in [20].

### III. RESULTS AND COMPARISON

The Gamow-Teller strength distributions,  $B(GT_\pm)$ , for  $^{24}\text{Mg}$  were calculated using the pn-QRPA theory. Quenching of the GT strength was taken into account and a standard quenching factor of 0.77 was used. The calculation was performed for a total of 132 excited states of  $^{24}\text{Mg}$  up to excitation energies in the vicinity of 40 MeV (corresponding to first 100 excited states) in the daughters  $^{24}\text{Na}$  and  $^{24}\text{Al}$ . The total calculated  $B(GT_+)$  and  $B(GT_-)$  strength came out to be 3.34 (quenched) and Ikeda sum rule was satisfied in the calculations.

In this section I present some of the results of the pn-QRPA calculated (anti)neutrino energy loss rates due to  $^{24}\text{Mg}$ . The reported rates are also compared against previous calculations.

Fig.1 and Fig. 2 show four panels depicting the calculated neutrino and antineutrino energy loss rates, respectively, at selected temperature and density domain. It is pertinent to mention again that the neutrino energy loss rates (depicted in Fig.1) contain contributions due to electron capture *and* positron decay on  $^{24}\text{Mg}$  whereas the antineutrino energy loss rates (Fig.2) are calculated due to contributions from positron capture *and* electron decay on  $^{24}\text{Mg}$ . The upper left panel, in both figures, shows the energy loss rates in low-density region ( $\rho[\text{gcm}^{-3}] = 10^{0.5}, 10^{1.5}$  and  $10^{2.5}$ ),

the upper right in medium-low density region ( $\rho[gcm^{-3}] = 10^{3.5}, 10^{4.5}$  and  $10^{5.5}$ ), the lower left in medium-high density region ( $\rho[gcm^{-3}] = 10^{6.5}, 10^{7.5}$  and  $10^{8.5}$ ) and finally the lower right panel depicts the calculated rates in high density region ( $\rho[gcm^{-3}] = 10^{9.5}, 10^{10.5}$  and  $10^{11}$ ). The (anti)neutrino energy loss rates are given in logarithmic scales (to base 10) in units of  $MeV.s^{-1}$ . In the figures  $T_9$  gives the stellar temperature in units of  $10^9$  K. One should note the order of magnitude differences in neutrino energy loss rates as the stellar temperature increases (Fig. 1). It can be seen from this figure that in the low density region the energy loss rates, as a function of stellar temperatures, are more or less superimposed on one another. This means that there is no appreciable change in the neutrino energy loss rates when increasing the density by an order of magnitude. There is a sharp exponential increase in the neutrino energy loss rates for the low, medium-low and medium-high density regions as the stellar temperature increases to  $T_9 = 5$ . Beyond this temperature the slope of the rates reduces drastically. One also observes that the neutrino energy loss rates are almost the same for the densities in the range  $(10 - 10^6)g/cm^3$  as a function of stellar temperature. For a given temperature the neutrino energy loss rates increase monotonically with increasing densities.

As far as the antineutrino energy loss rates are concerned (Fig. 2) one again notes that the rates increase very sharply as  $T_9$  approaches 5. The rates are again almost superimposed on one another as a function of stellar densities. However as the stellar matter moves from the medium high density region to high density region these rates start to 'peel off' from one another. The antineutrino production rates are dominated by the capture of positrons due to  $^{24}Mg$  with a relatively smaller contribution coming from the beta-decay of  $^{24}Mg$  (see Eq. (8)).

The current calculation was also compared with two earlier calculations of neutrino and antineutrino energy loss rates due to  $^{24}Mg$ . Fuller, Fowler and Newman [36] (hereafter FFN) compiled the experimental data and calculated neutrino and antineutrino energy loss rates (besides other weak-interaction mediated rates) for the nuclei in the mass range  $A = 21-60$  for an extended grid of temperature and density. The GT strength and excitation energies were calculated using a zero-order shell model. For the discrete transitions, for which the  $ft$  values were not available, FFN took  $\log ft = 5.0$ . Later Oda et al. [26] did an extensive calculation of stellar weak interaction rates of  $sd$ -shell nuclei in full  $(sd)^n$ -shell model space. They used the effective interaction of Wildenthal [17] and the available experimental compilations for their calculations.

Fig.3 (Fig.4) depicts the comparison of the pn-QRPA neutrino (antineutrino) energy loss rates with those calculated using shell model (OHMTS) [26] and those by FFN [36]. The ordinate represents the log (to base 10) of the calculated energy loss rates in units of  $MeV/s$ . The left panel depicts the different calculated energy loss rates at density  $10^3gcm^{-3}$ , the middle panel at density  $10^7gcm^{-3}$  and the right panel at density  $10^{11}gcm^{-3}$ . The shell model rates



are usually in good comparison with the corresponding FFN rates. The calculated pn-QRPA rates are enhanced. Table I shows the ratio of the calculated neutrino energy loss rates to those of Oda et al. [26] and FFN [36] calculations. In the table  $R_\nu(QRPA/OHMTS)$  denotes the ratio of the reported neutrino energy loss rates to those calculated using the shell model whereas  $R_\nu(QRPA/FFN)$  gives the corresponding ratio for the FFN calculations. The reported rates are more than a factor 15 enhanced as compared to the shell model rates in the presupernova conditions. The shell model rates are slightly enhanced at  $T_9 = 30$  (at high densities the pn-QRPA neutrino energy loss rates again surpass the shell model rates). The collapse simulators should take note of this enhanced neutrino energy loss rates which favor cooler cores with a lower entropy. It is important to note from Table I that, in comparison to previous calculations, the QRPA rates are most enhanced around  $T_9 \sim 1.5 - 2$  (i.e. during the presupernova evolution of O+Ne+Mg cores). The ratio then starts decreasing with increasing  $T_9$ . The enhancement of the QRPA rates around  $T_9 \sim 1.5 - 2$  may be traced back to the enhanced electron capture rates on  $^{24}\text{Mg}$  [37] leading to an enhanced production of non-thermal neutrinos around these temperatures. It may also be seen from Table I that at high temperatures ( $T_9 \sim 30$ ) the ratios are in good agreement with previous calculations.

The story is different for the comparison of antineutrino energy loss rates (Fig.4). This time the shell model rates and FFN rates are much more enhanced compared to pn-QRPA calculations. Nevertheless the antineutrino energy loss rates are very small numbers and can change by orders of magnitude by a mere change of 0.5 MeV, or less, in parent or daughter excitation energies and are more indicative of the uncertainties present in the calculation of the excitation energies.

Table II finally presents the calculated neutrino and antineutrino energy loss rates due to  $^{24}\text{Mg}$  on a detailed temperature-density grid suitable for simulation purposes. Here Column 1 shows the stellar density in logarithmic scales to base 10 (in units of  $gcm^{-3}$ ), Column 2 the stellar temperature in units of  $10^9 K$ . Stated also are the values of the Fermi energy of electrons in units of  $MeV$  in Column 3 whereas Column 4 and Column 5 display the corresponding calculated neutrino and antineutrino energy loss rates, respectively, in logarithmic scales to base 10 (in units of  $MeV.sec^{-1}$ ). The ASCII file of Table II is also available and can be received from the author upon request.

#### IV. CONCLUSIONS

There exists a wide variety of discrepant results in the supernova simulations of O+Ne+Mg cores including prompt explosions, delayed explosions and no explosions. Varying results of the simulations of O+Ne+Mg cores ask for a more careful analysis of the precollapse evolution. A large number of input parameters are required for these simulations

to run and a reliable calculation of these parameters can certainly reduce the large uncertainties involved. Neutrino energy loss rates are one of the key input nuclear physics parameters responsible for cooling the stellar cores and thereby reducing its entropy. The pn-QRPA calculations of the neutrino energy loss rates due to  $^{24}\text{Mg}$  are presented here on a detailed temperature-density grid suitable for simulation codes. The pn-QRPA calculations gives similar accuracy in reproducing weak interaction mediated rates in *sd*-shell nuclide [18] and is employed here using maximum possible experimental incorporations to further increase the reliability of the calculated numbers.

Recent simulations of O+Ne+Mg cores [15,16] employ the weak interaction rates of shell model [38,26], respectively. The reported neutrino energy loss rates are up to a factor of 15 enhanced as compared to shell model results. These enhanced numbers favor cooler cores with lower entropies. Can the enhanced reported neutrino energy loss rates lead to any change in the outcome of simulation results on O+Ne+Mg cores? Let us recall that in the simulations neutrino heating is a favored mechanism for revival of the stalled shock wave. The reported neutrino energy loss rates due to  $^{24}\text{Mg}$  and other nuclei of astrophysical importance (see e.g. Ref. [32]) employed preferably in a multi-dimensional model, with neutrino transport included consistently throughout the entire mass, accounting also for a complete treatment of multidimensional convection and burning phases might lead to some interesting outcome and answers.

## ACKNOWLEDGMENTS

The author would like to acknowledge the local hospitality provided by the Abdus Salam ICTP, Trieste, where part of this project was completed.

- 
- [1] S. A. Colgate and R. White, *Astrophys. J.* **143**, 626. (1966).
  - [2] W. D. Arnett, *Canadian J. Phys.* **45**, 1621 (1967).
  - [3] W. C. Haxton, *Phys. Rev. Lett.* **60**, 1999 (1988).
  - [4] S. W. Bruenn and W. C. Haxton, *Astrophys. J.* **376**, 678 (1991).
  - [5] K. Langanke, G. Martínez-Pinedo, B. Müller, H.-Th Janka, A. Marek, W. R. Hix, A. Juodagalvis, and J. M. Sampaio, *Phys. Rev. Lett.* **100**, 011101 (2008).
  - [6] W. Haxton, private communication.
  - [7] L. Dessart, A. Burrows, E. Livne, and C. D. Ott, *Astrophys. J.* **669**, 585 (2007).
  - [8] L. Dessart, A. Burrows, C. D. Ott, E. Livne, S.-Y. Yoon, and N. Langer, *Astrophys. J.* **644**, 1063 (2006).
  - [9] K. Nomoto and Y. Kondo, *Astrophys. J.* **367**, L19 (1991).
  - [10] K. Nomoto, *Astrophys. J.* **277**, 791 (1984).

- [11] W. Hillebrandt, K. Nomoto, and G. Wolff, *Astron. Astrophys.* **133**, 175 (1984).
- [12] S. E. Woosley and E. Baron, *Astrophys. J.* **391**, 228 (1992).
- [13] R. Mayle and J. R. Wilson, *Astrophys. J.* **334**, 909 (1988).
- [14] J. C. Wheeler, J. J. Cowan, and W. Hillebrandt, *Astrophys. J.* **493**, L101 (1998).
- [15] J. Gutiérrez, R. Canal, and E. García-Berro, *Astron. Astrophys.* **435**, 231 (2005).
- [16] F. S. Kitaura, H.-Th. Janka, and W. Hillebrandt, *Astron. Astrophys.* **450**, 345 (2006).
- [17] B. H. Wildenthal, M. S. Curtin, and B. A. Brown, *Phys. Rev. C* **28**, 1343 (1983).
- [18] A. Staudt, E. Bender, K. Muto, and H. V. Klapdor-Kleingrothaus, *At. Data Nucl. Data Tables* **44**, 79 (1990).
- [19] J.-U. Nabi and H. V. Klapdor-Kleingrothaus, *Eur. Phys. J. A* **5**, 337 (1999).
- [20] J.-U. Nabi and H. V. Klapdor-Kleingrothaus, *At. Data Nucl. Data Tables* **71**, 149 (1999).
- [21] J.-U. Nabi and H. V. Klapdor-Kleingrothaus, *At. Data Nucl. Data Tables* **88**, 237 (2004).
- [22] J.-U. Nabi and M.-U. Rahman, *Phys. Lett.* **B612**, 190 (2005).
- [23] J.-U. Nabi and M.-U. Rahman, *Phys. Rev. C* **75**, 035803 (2007).
- [24] J.-U. Nabi and M. Sajjad, *Phys. Rev. C* **76**, 055803 (2007).
- [25] J.-U. Nabi, M. Sajjad, and M.-U. Rahman, *Acta. Phys. Polon. B* **38**, 2665 (2007).
- [26] T. Oda, M. Hino, K. Muto, M. Takahara, and K. Sato, *At. Data Nucl. Data Tables* **56**, 231 (1994).
- [27] I. Stetcu and C. W. Johnson, *Phys. Rev. C* **69**, 024311 (2004).
- [28] S. Raman, C. H. Malarkey, W. T. Milner, C. W. Nestor Jr., and P. H. Stelson, *At. Data Nucl. Data Tables* **36**, 1 (1987).
- [29] M. Hirsch, A. Staudt, K. Muto, and H. V. Klapdor-Kleingrothaus, *At. Data Nucl. Data Tables* **53**, 165 (1993).
- [30] M. Hirsch, A. Staudt, K. Muto, and H. V. Klapdor-Kleingrothaus, *Nucl. Phys.* **A535**, 62 (1991).
- [31] G. Audi, A. H. Wapstra, and C. Thibault, *Nucl. Phys.* **A729**, 337 (2003).
- [32] J.-U. Nabi and M. Sajjad, *Phys. Rev. C* **77**, 055802 (2008).
- [33] G. P. Yost *et al.* (Particle Data Group), *Phys. Lett.* **B204**, 1 (1988).
- [34] V. Rodin, A. Faessler, F. Simkovic, and P. Vogel, *Czech. J. Phys.* **56**, 495 (2006).
- [35] N. B. Gove and M. J. Martin, *At. Data Nucl. Data Tables* **10**, 205 (1971).
- [36] G. M. Fuller, W. A. Fowler, and M. J. Newman, *Astrophys. J. Suppl. Ser* **42**, 447 (1980); **48**, 279 (1982); *Astrophys. J.* **252**, 715 (1982); **293**, 1 (1985).
- [37] J.-U. Nabi, *Phys. Scripta* (2008).
- [38] M. Takahara, M. Hino, T. Oda, K. Muto, A. A. Wolters, P. W. M. Glaudemans, and K. Sato, *Nucl. Phys.* **A504**, 167 (1989).

**Table I:** Ratios of QRPA calculated neutrino energy loss rates (due to  $^{24}\text{Mg}$ ) to those of OHMTS [26] and FFN [36]. First column gives the grid point, containing the log (to base 10) of stellar density and temperature in units of  $\text{gcm}^{-3}$  and  $10^9 \text{ K}$ , respectively, at which these rates were calculated.

$(\log(\rho Y_e), T_9)$	$R_\nu(QRPA/OHMTS)$	$R_\nu(QRPA/FFN)$
(1,1)	1.24E+01	1.13E+01
(1,1.5)	1.48E+01	1.14E+01
(1,2)	1.48E+01	9.84E+00
(1,3)	1.13E+01	7.01E+00
(1,5)	5.51E+00	3.91E+00
(1,10)	1.69E+00	1.95E+00
(1,30)	7.14E-01	1.61E+00
(3,1)	1.24E+01	1.13E+01
(3,1.5)	1.48E+01	1.14E+01
(3,2)	1.48E+01	9.84E+00
(3,3)	1.13E+01	7.01E+00
(3,5)	5.52E+00	3.92E+00
(3,10)	1.69E+00	1.95E+00
(3,30)	7.16E-01	1.61E+00
(7,1)	6.71E+00	5.98E+00
(7,1.5)	1.27E+01	9.68E+00
(7,2)	1.41E+01	9.35E+00
(7,3)	1.14E+01	7.05E+00
(7,5)	5.85E+00	4.08E+00
(7,10)	1.71E+00	1.96E+00
(7,30)	7.16E-01	1.62E+00
(11,1)	3.86E+00	3.80E+00
(11,1.5)	3.87E+00	3.79E+00
(11,2)	3.86E+00	3.78E+00
(11,3)	3.84E+00	3.67E+00
(11,5)	3.60E+00	3.24E+00
(11,10)	2.90E+00	2.20E+00
(11,30)	1.28E+00	1.77E+00

**Table II:** Calculated neutrino and antineutrino energy loss rates due to  $^{24}\text{Mg}$  for different selected densities and temperatures in stellar matter.  $\log(\rho Y_e)$  has units of  $\text{gcm}^{-3}$ , where  $\rho$  is the baryon density and  $Y_e$  is the ratio of the electron number to the baryon number. Temperatures ( $T_9$ ) are measured in  $10^9$  K.  $E_f$  is the total Fermi energy of electrons including the rest mass ( $\text{MeV}$ ).  $\lambda^\nu$  are the total neutrino energy loss rates ( $\text{MeVs}^{-1}$ ) due to  $\beta^+$  decay and electron capture on  $^{24}\text{Mg}$ .  $\lambda^{\bar{\nu}}$  are the total antineutrino energy loss rates ( $\text{MeVs}^{-1}$ ) due to  $\beta^-$  decay and positron capture on  $^{24}\text{Mg}$ . The calculated rates are tabulated in logarithmic (to base 10) scale. In the table, -100 means that the rate is smaller than  $10^{-100}$ .

$\log \rho Y_e$	$T_9$	$E_f$	$\lambda^\nu$	$\lambda^{\bar{\nu}}$	$\log \rho Y_e$	$T_9$	$E_f$	$\lambda^\nu$	$\lambda^{\bar{\nu}}$	$\log \rho Y_e$	$T_9$	$E_f$	$\lambda^\nu$	$\lambda^{\bar{\nu}}$
0.5	0.5	0.065	-66.886	-100	1	8.5	0	-3.497	-7.357	2	4.5	0	-8.258	-15.941
0.5	1	0	-35.745	-73.995	1	9	0	-3.156	-6.785	2	5	0	-7.319	-14.173
0.5	1.5	0	-24.62	-49.582	1	9.5	0	-2.843	-6.267	2	5.5	0	-6.529	-12.71
0.5	2	0	-18.795	-37.182	1	10	0	-2.555	-5.795	2	6	0	-5.851	-11.477
0.5	2.5	0	-15.167	-29.65	1	15	0	-0.505	-2.612	2	6.5	0	-5.263	-10.422
0.5	3	0	-12.667	-24.573	1	20	0	0.773	-0.8	2	7	0	-4.745	-9.506
0.5	3.5	0	-10.825	-20.907	1	25	0	1.697	0.427	2	7.5	0	-4.284	-8.703
0.5	4	0	-9.401	-18.128	1	30	0	2.416	1.341	2	8	0	-3.871	-7.992
0.5	4.5	0	-8.26	-15.942	1.5	0.5	0.162	-65.908	-100	2	8.5	0	-3.496	-7.356
0.5	5	0	-7.321	-14.175	1.5	1	0.002	-35.737	-74.001	2	9	0	-3.155	-6.784
0.5	5.5	0	-6.531	-12.712	1.5	1.5	0	-24.618	-49.582	2	9.5	0	-2.842	-6.266
0.5	6	0	-5.854	-11.479	1.5	2	0	-18.794	-37.182	2	10	0	-2.554	-5.794
0.5	6.5	0	-5.265	-10.424	1.5	2.5	0	-15.166	-29.65	2	15	0	-0.504	-2.611
0.5	7	0	-4.747	-9.508	1.5	3	0	-12.666	-24.572	2	20	0	0.774	-0.799
0.5	7.5	0	-4.287	-8.705	1.5	3.5	0	-10.824	-20.906	2	25	0	1.698	0.429
0.5	8	0	-3.873	-7.994	1.5	4	0	-9.399	-18.126	2	30	0	2.417	1.343
0.5	8.5	0	-3.499	-7.359	1.5	4.5	0	-8.259	-15.941	2.5	0.5	0.261	-64.907	-100
0.5	9	0	-3.158	-6.787	1.5	5	0	-7.319	-14.173	2.5	1	0.015	-35.669	-74.07
0.5	9.5	0	-2.845	-6.269	1.5	5.5	0	-6.529	-12.711	2.5	1.5	0.002	-24.613	-49.586
0.5	10	0	-2.557	-5.797	1.5	6	0	-5.852	-11.478	2.5	2	0	-18.793	-37.183
0.5	15	0	-0.507	-2.615	1.5	6.5	0	-5.263	-10.422	2.5	2.5	0	-15.165	-29.65
0.5	20	0	0.77	-0.803	1.5	7	0	-4.745	-9.506	2.5	3	0	-12.666	-24.572
0.5	25	0	1.694	0.424	1.5	7.5	0	-4.284	-8.703	2.5	3.5	0	-10.823	-20.906
0.5	30	0	2.412	1.337	1.5	8	0	-3.871	-7.992	2.5	4	0	-9.399	-18.126
1	0.5	0.113	-66.406	-100	1.5	8.5	0	-3.496	-7.356	2.5	4.5	0	-8.258	-15.941
1	1	0	-35.742	-73.996	1.5	9	0	-3.155	-6.784	2.5	5	0	-7.319	-14.173
1	1.5	0	-24.619	-49.582	1.5	9.5	0	-2.843	-6.266	2.5	5.5	0	-6.528	-12.71
1	2	0	-18.794	-37.182	1.5	10	0	-2.554	-5.794	2.5	6	0	-5.851	-11.477
1	2.5	0	-15.166	-29.65	1.5	15	0	-0.504	-2.611	2.5	6.5	0	-5.263	-10.422
1	3	0	-12.666	-24.572	1.5	20	0	0.774	-0.799	2.5	7	0	-4.745	-9.506
1	3.5	0	-10.824	-20.906	1.5	25	0	1.698	0.428	2.5	7.5	0	-4.284	-8.703
1	4	0	-9.4	-18.127	1.5	30	0	2.416	1.342	2.5	8	0	-3.87	-7.991
1	4.5	0	-8.259	-15.941	2	0.5	0.212	-65.408	-100	2.5	8.5	0	-3.496	-7.356
1	5	0	-7.32	-14.174	2	1	0.005	-35.72	-74.018	2.5	9	0	-3.155	-6.784
1	5.5	0	-6.529	-12.711	2	1.5	0	-24.617	-49.583	2.5	9.5	0	-2.842	-6.266
1	6	0	-5.852	-11.478	2	2	0	-18.793	-37.182	2.5	10	0	-2.554	-5.794
1	6.5	0	-5.264	-10.422	2	2.5	0	-15.166	-29.65	2.5	15	0	-0.504	-2.611
1	7	0	-4.746	-9.507	2	3	0	-12.666	-24.572	2.5	20	0	0.774	-0.799
1	7.5	0	-4.285	-8.704	2	3.5	0	-10.824	-20.906	2.5	25	0	1.698	0.429
1	8	0	-3.871	-7.992	2	4	0	-9.399	-18.126	2.5	30	0	2.417	1.343

$\log \rho Y_e$	$T_9$	$E_f$	$\lambda^\nu$	$\lambda^{\bar{\nu}}$	$\log \rho Y_e$	$T_9$	$E_f$	$\lambda^\nu$	$\lambda^{\bar{\nu}}$	$\log \rho Y_e$	$T_9$	$E_f$	$\lambda^\nu$	$\lambda^{\bar{\nu}}$
3	0.5	0.311	-64.406	-100	4	0.5	0.411	-63.394	-100	5	0.5	0.522	-62.276	-100
3	1	0.046	-35.514	-74.224	4	1	0.209	-34.692	-75.046	5	1	0.413	-33.661	-76.078
3	1.5	0.005	-24.602	-49.597	4	1.5	0.047	-24.461	-49.739	5	1.5	0.265	-23.727	-50.473
3	2	0.001	-18.79	-37.185	4	2	0.014	-18.759	-37.216	5	2	0.128	-18.47	-37.505
3	2.5	0.001	-15.165	-29.651	4	2.5	0.006	-15.153	-29.662	5	2.5	0.062	-15.041	-29.775
3	3	0	-12.665	-24.572	4	3	0.004	-12.66	-24.578	5	3	0.035	-12.606	-24.631
3	3.5	0	-10.823	-20.906	4	3.5	0.002	-10.82	-20.909	5	3.5	0.023	-10.791	-20.938
3	4	0	-9.399	-18.126	4	4	0.002	-9.397	-18.128	5	4	0.016	-9.379	-18.146
3	4.5	0	-8.258	-15.941	4	4.5	0.001	-8.257	-15.942	5	4.5	0.012	-8.245	-15.954
3	5	0	-7.319	-14.173	4	5	0.001	-7.318	-14.174	5	5	0.009	-7.31	-14.182
3	5.5	0	-6.528	-12.71	4	5.5	0.001	-6.528	-12.711	5	5.5	0.007	-6.522	-12.717
3	6	0	-5.851	-11.477	4	6	0.001	-5.851	-11.478	5	6	0.006	-5.846	-11.482
3	6.5	0	-5.263	-10.422	4	6.5	0.001	-5.262	-10.422	5	6.5	0.005	-5.259	-10.425
3	7	0	-4.745	-9.506	4	7	0	-4.744	-9.506	5	7	0.004	-4.742	-9.509
3	7.5	0	-4.284	-8.703	4	7.5	0	-4.284	-8.703	5	7.5	0.004	-4.281	-8.705
3	8	0	-3.87	-7.991	4	8	0	-3.87	-7.991	5	8	0.003	-3.868	-7.993
3	8.5	0	-3.496	-7.356	4	8.5	0	-3.496	-7.356	5	8.5	0.003	-3.494	-7.357
3	9	0	-3.155	-6.784	4	9	0	-3.155	-6.784	5	9	0.002	-3.153	-6.785
3	9.5	0	-2.842	-6.266	4	9.5	0	-2.842	-6.266	5	9.5	0.002	-2.841	-6.267
3	10	0	-2.554	-5.794	4	10	0	-2.554	-5.794	5	10	0.002	-2.553	-5.794
3	15	0	-0.503	-2.611	4	15	0	-0.503	-2.61	5	15	0.001	-0.503	-2.611
3	20	0	0.775	-0.799	4	20	0	0.775	-0.799	5	20	0	0.775	-0.799
3	25	0	1.699	0.429	4	25	0	1.699	0.429	5	25	0	1.699	0.429
3	30	0	2.417	1.343	4	30	0	2.417	1.343	5	30	0	2.417	1.343
3.5	0.5	0.361	-63.904	-100	4.5	0.5	0.464	-62.865	-100	5.5	0.5	0.598	-61.518	-100
3.5	1	0.115	-35.167	-74.571	4.5	1	0.309	-34.187	-75.552	5.5	1	0.528	-33.082	-76.657
3.5	1.5	0.015	-24.568	-49.632	4.5	1.5	0.13	-24.182	-50.017	5.5	1.5	0.423	-23.198	-51.003
3.5	2	0.004	-18.783	-37.192	4.5	2	0.044	-18.683	-37.292	5.5	2	0.295	-18.049	-37.926
3.5	2.5	0.002	-15.162	-29.653	4.5	2.5	0.02	-15.126	-29.689	5.5	2.5	0.18	-14.803	-30.013
3.5	3	0.001	-12.664	-24.574	4.5	3	0.011	-12.647	-24.591	5.5	3	0.11	-12.482	-24.756
3.5	3.5	0.001	-10.822	-20.907	4.5	3.5	0.007	-10.813	-20.916	5.5	3.5	0.072	-10.72	-21.009
3.5	4	0.001	-9.398	-18.127	4.5	4	0.005	-9.393	-18.132	5.5	4	0.05	-9.336	-18.19
3.5	4.5	0	-8.258	-15.941	4.5	4.5	0.004	-8.254	-15.945	5.5	4.5	0.038	-8.216	-15.983
3.5	5	0	-7.319	-14.173	4.5	5	0.003	-7.316	-14.176	5.5	5	0.029	-7.29	-14.202
3.5	5.5	0	-6.528	-12.71	4.5	5.5	0.002	-6.526	-12.712	5.5	5.5	0.023	-6.507	-12.731
3.5	6	0	-5.851	-11.477	4.5	6	0.002	-5.85	-11.479	5.5	6	0.019	-5.835	-11.493
3.5	6.5	0	-5.263	-10.422	4.5	6.5	0.002	-5.261	-10.423	5.5	6.5	0.016	-5.25	-10.434
3.5	7	0	-4.745	-9.506	4.5	7	0.001	-4.744	-9.507	5.5	7	0.013	-4.735	-9.515
3.5	7.5	0	-4.284	-8.703	4.5	7.5	0.001	-4.283	-8.703	5.5	7.5	0.012	-4.276	-8.71
3.5	8	0	-3.87	-7.991	4.5	8	0.001	-3.87	-7.992	5.5	8	0.01	-3.864	-7.998
3.5	8.5	0	-3.496	-7.356	4.5	8.5	0.001	-3.495	-7.356	5.5	8.5	0.009	-3.491	-7.361
3.5	9	0	-3.155	-6.784	4.5	9	0.001	-3.154	-6.784	5.5	9	0.008	-3.151	-6.788
3.5	9.5	0	-2.842	-6.266	4.5	9.5	0.001	-2.842	-6.266	5.5	9.5	0.007	-2.838	-6.269
3.5	10	0	-2.554	-5.794	4.5	10	0.001	-2.553	-5.794	5.5	10	0.006	-2.55	-5.797
3.5	15	0	-0.503	-2.61	4.5	15	0	-0.503	-2.61	5.5	15	0.003	-0.502	-2.611
3.5	20	0	0.775	-0.799	4.5	20	0	0.775	-0.799	5.5	20	0.001	0.775	-0.799
3.5	25	0	1.699	0.429	4.5	25	0	1.699	0.429	5.5	25	0.001	1.699	0.429
3.5	30	0	2.417	1.343	4.5	30	0	2.417	1.343	5.5	30	0.001	2.418	1.343

$\log \rho Y_e$	$T_9$	$E_f$	$\lambda^\nu$	$\lambda^{\bar{\nu}}$	$\log \rho Y_e$	$T_9$	$E_f$	$\lambda^\nu$	$\lambda^{\bar{\nu}}$	$\log \rho Y_e$	$T_9$	$E_f$	$\lambda^\nu$	$\lambda^{\bar{\nu}}$
6	0.5	0.713	-60.357	-100	7	0.5	1.217	-56.685	-100	8	0.5	2.444	-46.023	-100
6	1	0.672	-32.361	-77.381	7	1	1.2	-29.976	-80.038	8	1	2.437	-24.4	-85.748
6	1.5	0.604	-22.592	-51.61	7	1.5	1.173	-20.755	-53.519	8	1.5	2.424	-16.885	-57.677
6	2	0.512	-17.504	-38.473	7	2	1.133	-15.966	-40.037	8	2	2.406	-12.964	-43.235
6	2.5	0.405	-14.351	-30.465	7	2.5	1.083	-12.997	-31.832	8	2.5	2.383	-10.511	-34.45
6	3	0.299	-12.164	-25.074	7	3	1.021	-10.959	-26.287	8	3	2.355	-8.812	-28.526
6	3.5	0.214	-10.515	-21.214	7	3.5	0.95	-9.461	-22.274	8	3.5	2.322	-7.553	-24.248
6	4	0.156	-9.203	-18.323	7	4	0.871	-8.307	-19.223	8	4	2.283	-6.577	-21.003
6	4.5	0.117	-8.127	-16.072	7	4.5	0.785	-7.382	-16.82	8	4.5	2.24	-5.792	-18.449
6	5	0.091	-7.227	-14.265	7	5	0.698	-6.618	-14.877	8	5	2.192	-5.144	-16.382
6	5.5	0.073	-6.461	-12.777	7	5.5	0.613	-5.969	-13.272	8	5.5	2.139	-4.597	-14.67
6	6	0.06	-5.801	-11.527	7	6	0.534	-5.404	-11.926	8	6	2.081	-4.127	-13.225
6	6.5	0.05	-5.224	-10.46	7	6.5	0.465	-4.904	-10.782	8	6.5	2.019	-3.718	-11.987
6	7	0.042	-4.714	-9.536	7	7	0.404	-4.455	-9.797	8	7	1.952	-3.357	-10.911
6	7.5	0.036	-4.259	-8.727	7	7.5	0.353	-4.048	-8.94	8	7.5	1.882	-3.034	-9.967
6	8	0.032	-3.85	-8.011	7	8	0.31	-3.676	-8.187	8	8	1.808	-2.744	-9.13
6	8.5	0.028	-3.479	-7.372	7	8.5	0.274	-3.334	-7.518	8	8.5	1.732	-2.481	-8.382
6	9	0.025	-3.141	-6.798	7	9	0.244	-3.019	-6.92	8	9	1.653	-2.239	-7.71
6	9.5	0.022	-2.83	-6.277	7	9.5	0.218	-2.727	-6.381	8	9.5	1.574	-2.016	-7.1
6	10	0.02	-2.544	-5.803	7	10	0.196	-2.455	-5.892	8	10	1.493	-1.809	-6.546
6	15	0.009	-0.5	-2.613	7	15	0.085	-0.475	-2.639	8	15	0.817	-0.231	-2.885
6	20	0.005	0.776	-0.8	7	20	0.047	0.787	-0.81	8	20	0.47	0.892	-0.917
6	25	0.003	1.699	0.429	7	25	0.03	1.705	0.423	8	25	0.301	1.759	0.369
6	30	0.002	2.418	1.343	7	30	0.021	2.421	1.34	8	30	0.209	2.452	1.309
6.5	0.5	0.905	-58.556	-100	7.5	0.5	1.705	-53.469	-100	8.5	0.5	3.547	-34.902	-100
6.5	1	0.88	-31.345	-78.427	7.5	1	1.693	-28.044	-82.349	8.5	1	3.542	-18.828	-91.319
6.5	1.5	0.837	-21.819	-52.393	7.5	1.5	1.675	-19.269	-55.187	8.5	1.5	3.534	-13.164	-61.405
6.5	2	0.777	-16.842	-39.139	7.5	2	1.648	-14.756	-41.33	8.5	2	3.521	-10.181	-46.046
6.5	2.5	0.701	-13.756	-31.062	7.5	2.5	1.614	-11.971	-32.902	8.5	2.5	3.506	-8.295	-36.714
6.5	3	0.612	-11.64	-25.6	7.5	3	1.573	-10.058	-27.214	8.5	3	3.487	-6.971	-30.428
6.5	3.5	0.517	-10.081	-21.65	7.5	3.5	1.524	-8.652	-23.1	8.5	3.5	3.464	-5.973	-25.893
6.5	4	0.424	-8.866	-18.66	7.5	4	1.468	-7.566	-19.976	8.5	4	3.438	-5.185	-22.457
6.5	4.5	0.343	-7.875	-16.324	7.5	4.5	1.405	-6.697	-17.515	8.5	4.5	3.408	-4.542	-19.758
6.5	5	0.277	-7.04	-14.452	7.5	5	1.336	-5.982	-15.52	8.5	5	3.375	-4.005	-17.575
6.5	5.5	0.226	-6.322	-12.917	7.5	5.5	1.262	-5.381	-13.866	8.5	5.5	3.339	-3.546	-15.769
6.5	6	0.187	-5.695	-11.634	7.5	6	1.183	-4.865	-12.47	8.5	6	3.299	-3.147	-14.248
6.5	6.5	0.157	-5.141	-10.543	7.5	6.5	1.101	-4.415	-11.275	8.5	6.5	3.256	-2.798	-12.945
6.5	7	0.134	-4.649	-9.602	7.5	7	1.018	-4.016	-10.239	8.5	7	3.209	-2.487	-11.816
6.5	7.5	0.115	-4.207	-8.78	7.5	7.5	0.937	-3.659	-9.332	8.5	7.5	3.159	-2.208	-10.825
6.5	8	0.1	-3.807	-8.054	7.5	8	0.858	-3.333	-8.532	8.5	8	3.106	-1.955	-9.948
6.5	8.5	0.088	-3.444	-7.408	7.5	8.5	0.783	-3.035	-7.82	8.5	8.5	3.05	-1.725	-9.164
6.5	9	0.078	-3.111	-6.827	7.5	9	0.714	-2.758	-7.184	8.5	9	2.99	-1.514	-8.458
6.5	9.5	0.069	-2.805	-6.302	7.5	9.5	0.651	-2.499	-6.611	8.5	9.5	2.928	-1.319	-7.819
6.5	10	0.062	-2.522	-5.825	7.5	10	0.593	-2.257	-6.092	8.5	10	2.863	-1.138	-7.236
6.5	15	0.027	-0.494	-2.619	7.5	15	0.268	-0.414	-2.7	8.5	15	2.109	0.195	-3.318
6.5	20	0.015	0.779	-0.802	7.5	20	0.15	0.812	-0.836	8.5	20	1.402	1.124	-1.152
6.5	25	0.01	1.701	0.428	7.5	25	0.095	1.718	0.41	8.5	25	0.936	1.885	0.241
6.5	30	0.007	2.419	1.342	7.5	30	0.066	2.428	1.332	8.5	30	0.656	2.527	1.233



$\log \rho Y_e$	$T_9$	$E_f$	$\lambda^\nu$	$\lambda^{\bar{\nu}}$	$\log \rho Y_e$	$T_9$	$E_f$	$\lambda^\nu$	$\lambda^{\bar{\nu}}$	$\log \rho Y_e$	$T_9$	$E_f$	$\lambda^\nu$	$\lambda^{\bar{\nu}}$
9	0.5	5.179	-18.453	-100	9.5	8.5	7.351	0.661	-11.712	10.5	4.5	16.28	3.848	-34.166
9	1	5.176	-10.596	-99.551	9.5	9	7.323	0.749	-10.883	10.5	5	16.273	3.848	-30.569
9	1.5	5.17	-7.666	-66.903	9.5	9.5	7.293	0.836	-10.133	10.5	5.5	16.265	3.847	-27.609
9	2	5.162	-6.048	-50.178	9.5	10	7.261	0.922	-9.452	10.5	6	16.256	3.846	-25.127
9	2.5	5.151	-4.983	-40.029	9.5	15	6.86	1.689	-4.914	10.5	6.5	16.247	3.845	-23.014
9	3	5.138	-4.208	-33.2	9.5	20	6.307	2.304	-2.387	10.5	7	16.237	3.845	-21.192
9	3.5	5.122	-3.607	-28.279	9.5	25	5.624	2.8	-0.704	10.5	7.5	16.226	3.845	-19.603
9	4	5.105	-3.119	-24.555	9.5	30	4.859	3.216	0.528	10.5	8	16.214	3.846	-18.203
9	4.5	5.085	-2.71	-21.633	10	0.5	11.118	2.13	-100	10.5	8.5	16.202	3.847	-16.959
9	5	5.062	-2.358	-19.273	10	1	11.116	2.133	-100	10.5	9	16.189	3.849	-15.847
9	5.5	5.037	-2.049	-17.324	10	1.5	11.113	2.139	-86.813	10.5	9.5	16.175	3.852	-14.844
9	6	5.01	-1.773	-15.684	10	2	11.11	2.146	-65.139	10.5	10	16.16	3.856	-13.936
9	6.5	4.98	-1.525	-14.281	10	2.5	11.105	2.154	-52.016	10.5	15	15.973	3.964	-7.976
9	7	4.948	-1.3	-13.067	10	3	11.099	2.164	-43.204	10.5	20	15.711	4.192	-4.757
9	7.5	4.914	-1.093	-12.003	10	3.5	11.091	2.175	-36.867	10.5	25	15.375	4.461	-2.669
9	8	4.878	-0.902	-11.063	10	4	11.083	2.186	-32.083	10.5	30	14.965	4.716	-1.17
9	8.5	4.839	-0.724	-10.224	10	4.5	11.074	2.198	-28.337	11	0.5	23.934	5.232	-100
9	9	4.797	-0.559	-9.469	10	5	11.063	2.21	-25.319	11	1	23.933	5.232	-100
9	9.5	4.754	-0.405	-8.787	10	5.5	11.052	2.224	-22.833	11	1.5	23.932	5.233	-100
9	10	4.708	-0.26	-8.165	10	6	11.039	2.238	-20.746	11	2	23.93	5.233	-97.44
9	15	4.131	0.848	-3.998	10	6.5	11.025	2.254	-18.967	11	2.5	23.928	5.233	-77.863
9	20	3.39	1.612	-1.652	10	7	11.011	2.27	-17.43	11	3	23.925	5.233	-64.749
9	25	2.621	2.219	-0.098	10	7.5	10.995	2.288	-16.088	11	3.5	23.922	5.231	-55.34
9	30	1.973	2.744	1.013	10	8	10.978	2.308	-14.904	11	4	23.918	5.229	-48.252
9.5	0.5	7.583	-0.829	-100	10	8.5	10.959	2.329	-13.852	11	4.5	23.913	5.226	-42.715
9.5	1	7.581	-0.787	-100	10	9	10.94	2.351	-12.908	11	5	23.908	5.222	-38.266
9.5	1.5	7.577	-0.721	-74.939	10	9.5	10.92	2.376	-12.057	11	5.5	23.903	5.218	-34.608
9.5	2	7.571	-0.637	-56.226	10	10	10.898	2.402	-11.284	11	6	23.897	5.214	-31.545
9.5	2.5	7.564	-0.541	-44.88	10	15	10.624	2.75	-6.179	11	6.5	23.891	5.209	-28.941
9.5	3	7.555	-0.437	-37.252	10	20	10.241	3.167	-3.378	11	7	23.884	5.205	-26.698
9.5	3.5	7.545	-0.329	-31.76	10	25	9.751	3.554	-1.536	11	7.5	23.877	5.2	-24.744
9.5	4	7.532	-0.221	-27.61	10	30	9.163	3.891	-0.195	11	8	23.869	5.196	-23.025
9.5	4.5	7.519	-0.114	-24.356	10.5	0.5	16.31	3.841	-100	11	8.5	23.86	5.192	-21.5
9.5	5	7.503	-0.009	-21.731	10.5	1	16.309	3.842	-100	11	9	23.851	5.188	-20.138
9.5	5.5	7.486	0.093	-19.566	10.5	1.5	16.307	3.843	-100	11	9.5	23.842	5.185	-18.912
9.5	6	7.468	0.193	-17.746	10.5	2	16.304	3.845	-78.224	11	10	23.832	5.182	-17.802
9.5	6.5	7.448	0.291	-16.193	10.5	2.5	16.301	3.846	-62.488	11	15	23.704	5.196	-10.574
9.5	7	7.426	0.386	-14.849	10.5	3	16.297	3.848	-51.934	11	20	23.526	5.309	-6.726
9.5	7.5	7.403	0.479	-13.674	10.5	3.5	16.292	3.848	-44.354	11	25	23.296	5.484	-4.266
9.5	8	7.378	0.571	-12.637	10.5	4	16.286	3.849	-38.637	11	30	23.016	5.669	-2.522

FIG. 1: (Color online) Neutrino energy loss rates due to  $^{24}\text{Mg}$ , as a function of stellar temperatures, for different selected stellar densities. Densities are given in units of  $gcm^{-3}$ . Temperatures are measured in  $10^9$  K and  $\log\lambda_\nu$  represents the log (to base 10) of neutrino energy loss rates in units of  $MeVsec^{-1}$ .

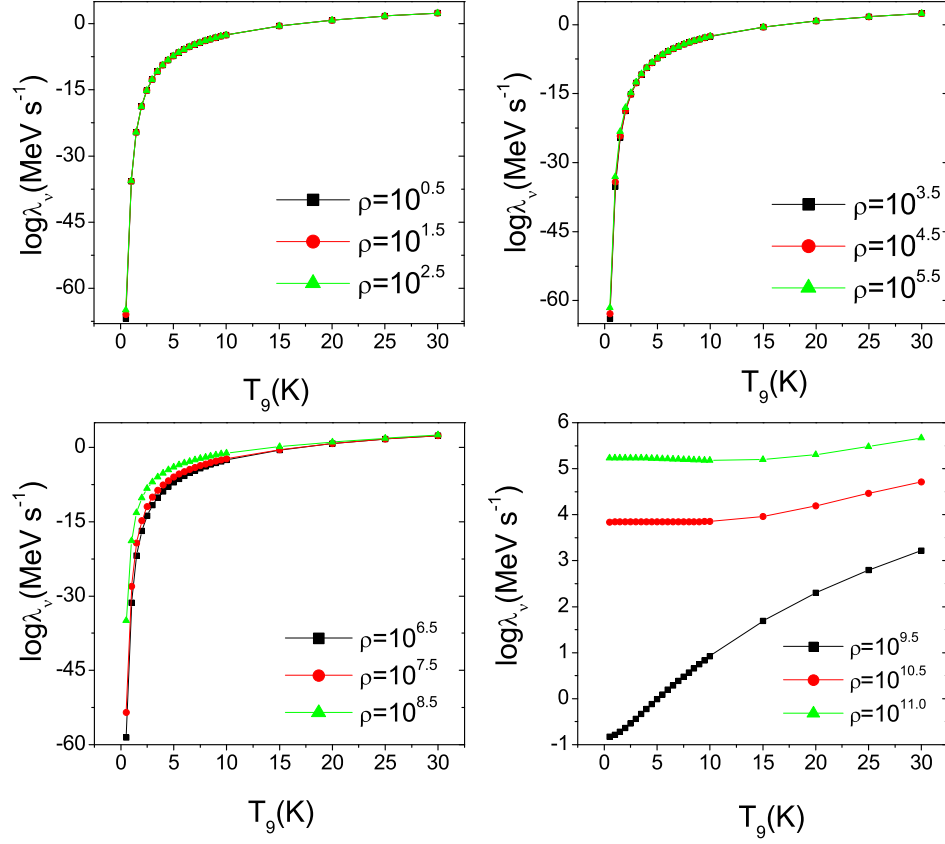


FIG. 2: (Color online) Same as Fig.1 but for antineutrino energy loss rates.

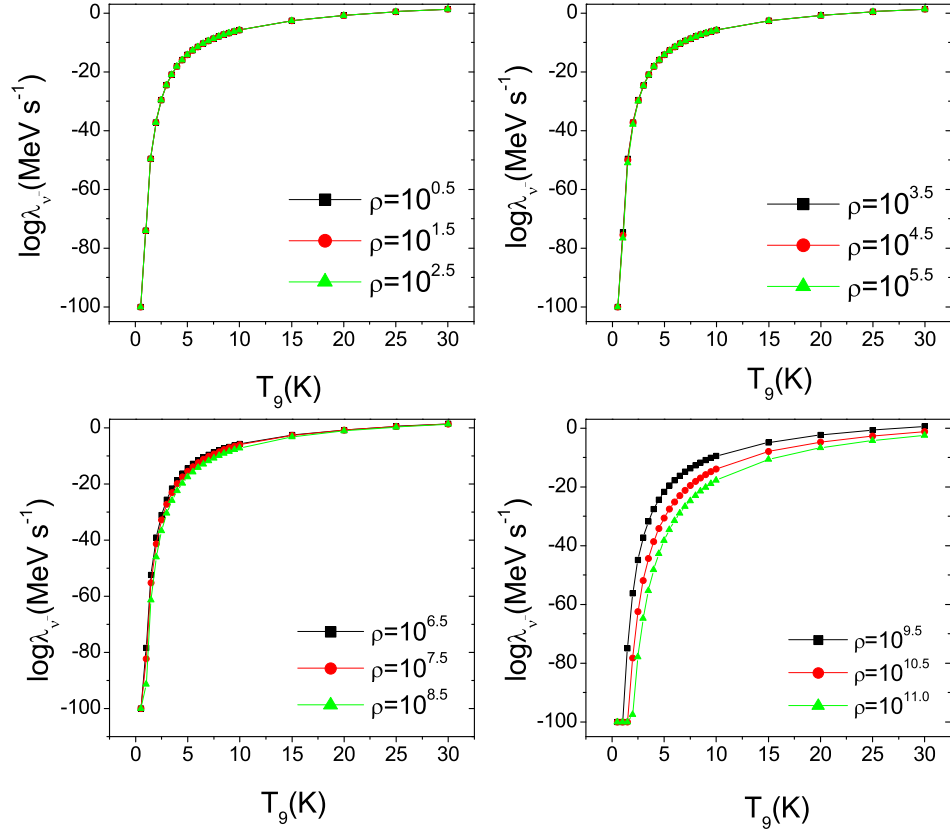


FIG. 3: (Color online) Comparison of pn-QRPA calculated neutrino energy loss rates with those calculated using shell model (OHMTS) [26] and those calculated by FFN [36] as a function of stellar temperatures and densities. Ordinate represents the log (to base 10) of neutrino energy loss rates in units of  $MeV sec^{-1}$ .

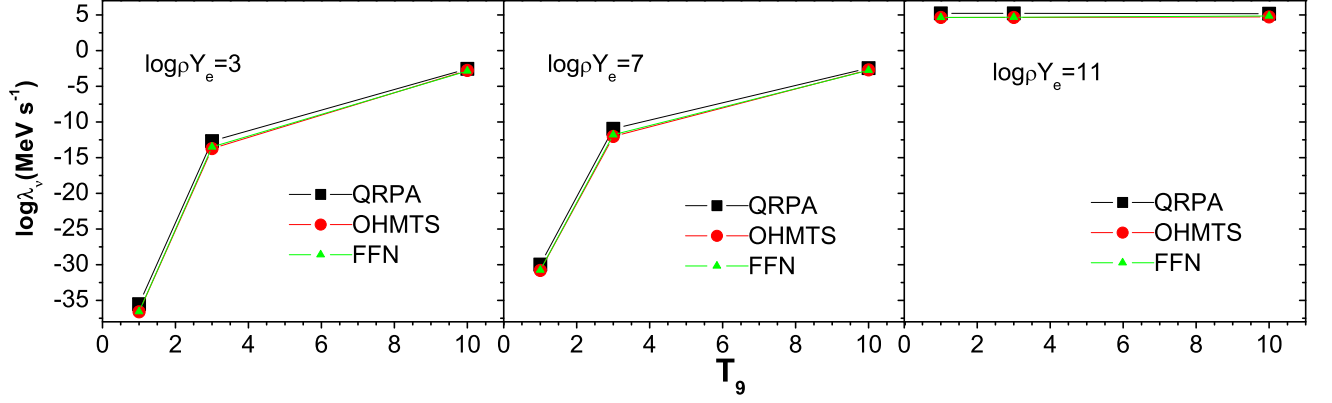


FIG. 4: (Color online) Same as Fig.3 but for antineutrino energy loss rates.

